

Decision Theory for the Mass Measurements at the Facility for Rare Isotope Beams

Jesse N. Farr¹, Zach Meisel², and Andrew W. Steiner¹

¹*Department of Physics and Astronomy, University of Tennessee, Knoxville, TN 37996, USA and*

²*Institute of Nuclear & Particle Physics, Department of Physics & Astronomy, Ohio University, Athens, OH, 45701 USA*

Nuclear physics facilities, like the Facility for Rare Isotope Beams (FRIB), can potentially perform many nuclear mass measurements of exotic isotopes. Each measurement comes with a particular cost, both in time and money, and thus it is important to establish which mass measurements are the most informative. In this article, we show that one can use the Kullback-Leibler divergence to determine the information gained by a mass measurement. We model the information gain obtained by nuclear mass measurements from two perspectives: first from the perspective of theoretical nuclear mass models, and the second from the perspective of r-process nucleosynthesis. While this work specifically analyzes the abilities of FRIB, other facilities worldwide could benefit from a similar use of information gain in order to decide which experiments are optimal.

I. INTRODUCTION

There are thousands of isotopes accessible using nuclear physics facilities like the Facility for Rare Isotope Beams (FRIB), yet each experiment requires beam time and a considerable amount of human effort. Thus, it is worth attempting to quantify the information gained by performing an experiment relative to its cost. One mechanism for making that quantification is decision theory, where a utility function is maximized in order to make the best decision given a domain of problems under consideration. The utility function, however, is not uniquely determined. It depends on the nature of the facility, the results which have been obtained from previous facilities, and even the makeup of the team performing the next experiment.

We choose only to analyze nuclear mass measurements at FRIB, and leave the consideration of other facilities to future work. We also make the (strong) assumption that this cost is dominated by the beam time required to perform a mass measurement.

Given a prior probability distribution $P(x_1, x_2, \dots, x_k)$ defined over a domain X , and a resulting posterior distribution Q , the information contained in the posterior relative to the prior is the Kullback-Leibler (KL) divergence

$$D_{KL}(Q||P) = \sum_{x \in X} P(x) \ln \frac{P(x)}{Q(x)}. \quad (1)$$

If the posterior and prior are identical, then the KL divergence is zero. Under the additional assumption that both the prior and posterior distributions are multivariate Gaussians, the KL divergence is

$$D_{KL}(\mathcal{N}_Q||\mathcal{N}_P) = \frac{1}{2} \left[\text{tr}(\Sigma_P^{-1}\Sigma_Q) - k + \ln \left(\frac{\det \Sigma_P}{\det \Sigma_Q} \right) + (\mu_P - \mu_Q)^T \Sigma_P^{-1} (\mu_P - \mu_Q) \right] \quad (2)$$

where \mathcal{N}_P and \mathcal{N}_Q are the prior and posterior distributions, respectively, Σ_P and Σ_Q are the corresponding covariance matrices, μ_P and μ_Q are the means of the Gaussians, and k is the dimensionality of the space. In

the case of two one-dimensional Gaussians with identical means, the KL divergence is simply a function of the two standard deviations, i.e. $D_{KL}(\sigma_Q|\sigma_P)$ and the KL divergence depends only on the ratio of the two, σ_P/σ_Q .

The value of nuclear mass measurements, however, lies not only in the information contained in the masses themselves, but also in what those masses mean for theoretical models of nuclear structure or physical processes involving nuclei. Both of these applications come with their own information gain. In this work, we model the information gain obtained by nuclear mass measurements from two perspectives: first from the perspective of theoretical mass models as understood by mass tabulations, and the second from the perspective of r-process nucleosynthesis.

II. ESTIMATED MASS REACH

The two primary mass measurement techniques to be employed at FRIB are Penning trap mass spectrometry (PTMS) and time-of-flight mass spectrometry (TOFMS). PTMS is a high precision technique requiring stopped radioactive ion beams, while TOFMS is a lower precision technique that uses fast beams and is suited for nuclides with short half-lives or low production rates. Generally speaking, PTMS is used to establish a precise nuclear mass surface that TOFMS then extends to more exotic isotopes.

PTMS measurements at FRIB will be performed with the Low Energy Beam Ion Trap [1]. Several PTMS techniques exist. Here we consider the time-of-flight ion-cyclotron-resonance (TOF-ICR) technique, which is the most commonly used to date. For the TOF-ICR PTMS technique, the ion's cyclotron resonance is found and converted from the orbital motion into motion leaving the trap, which is proportional to the ion's mass. The relative statistical uncertainty $\delta m/m$ is roughly given by $\delta m/m \approx R^{-1}n^{-1/2}$, where n is the number of ions detected and R is the resolving power [2]. The resolving power is approximately equal to the product of the cyclotron frequency of the ion in the trap (typically \sim MHz)

and the length of time the ion orbits in the trap t_{obs} (typically ~ 0.1 s). R therefore depends on many considerations, such as the mass of the nucleus of interest, the obtainable charge-state, the time it takes to produce the optimum charge state, and the nuclear half-life. Given the uncertainties in charge-breeding capabilities and the approximate nature of the estimate for n , we assume $R = 10^5$, which is in-line with sample cases for rare isotopes [3]. Further, we assume a typical $t_{\text{obs}}=100$ ms, meaning that n is the product of the FRIB stopped-beam rate and the duration of the experiment, assumed to be 24 hours, reduced by the radioactive decay of ions during the measurement process. Experimental β -decay half-lives [4] are used when available and theory estimates [5] are used otherwise. The assumed systematic uncertainty is $\delta m/m|_{\text{syst}} = 10^{-8}$, which is typical for the measurement precision of reference ions used in a PTMS measurement [1].

TOFMS at FRIB will consist of TOF and magnetic rigidity measurements for ions traversing a several tens of meter flight path, e.g. as in Ref. [6]. The proportionality between rigidity-corrected TOF and nuclear mass is calibrated by simultaneously measuring nuclides with known masses, typically from prior PTMS measurements. The statistical uncertainty of TOFMS is related to the TOF measurement precision $\sigma_{\text{TOF}}/\text{TOF}$ and n , here based on the fast beam rate and 100 hours of measurement time, by $\delta m/m \approx \sigma_{\text{TOF}}/(\text{TOF}\sqrt{n})$, where we assume a typical $\sigma_{\text{TOF}}/\text{TOF}$ of 10^{-4} [7]. The systematic uncertainty that we adopt is based on the empirically motivated approximation that $\delta m/m|_{\text{syst}} = 5 \times 10^{-6}(1 + (N - N_{\text{ref}}))$, where $N - N_{\text{ref}}$ is the number of neutrons separating the nuclide of interest and the most neutron-rich isotope of that element with a known mass uncertainty $\leq 10^{-6}$ [7].

Using the estimated fast and stopped beam rates at FRIB [8], we calculate n . We then estimate $\delta m/m$ for PTMS and, for cases where this is greater than 10^{-6} , for TOFMS, up to cases with $\delta m/m = 10^{-4}$. The smaller of the two δm is used in the subsequent calculation of the KL divergence.

III. INFORMATION GAIN RELATIVE TO THEORETICAL MASS MODELS

For each nucleus which from the previous section which is accessible from FRIB, we presume that the associated probability distribution from theory is a Gaussian, given by the mean and the standard deviation of the theoretical predictions across mass models. Thus

$$\sigma_{\text{th}} = \sigma_{M(Z,N)}. \quad (3)$$

For the theoretical mass models, we use the masses from Chamel et al. (2009) [9], Dufflo et al. (2003) [10], Ebran et al. (2011) [11], Goriely et al. (2003, 2007, 2008, 2008b, 2010, 2014) [12–17], Koura et al. (2005) [18], Long et al. (2010) [19], Liu et al. (2011) [20], Moller et al. (2016) [21], Pearson et al. (2011) [22], Rath et al.

(2010) [23], and Wang et al. (2010, 2001b) [24, 25]. The decision to exclude other similar mass models was made in part due to the limited range of isotopes that the models cover. We have found that our results are relatively insensitive to the exact list of theoretical mass models.

Using these mass models, the standard deviation in the predicted nuclear mass, σ_{th} is plotted in the upper-left panel of Fig 1. (We include experimentally measured nuclei in this plot, even though for these nuclei the variation across mass models is best measured by the variation across experimental mass measurements rather than from theory.) The largest uncertainties between mass models occur at the edge of the neutron drip line very close to the $Z = 82$ shell. This result is not surprising; it is well-known that theoretical mass models have a difficult time correctly describing shell effects.

Given a nucleus, we assume that the experimental information obtained by a FRIB measurement is a Gaussian with a standard deviation of

$$\sigma_{\text{ex}} = \delta m. \quad (4)$$

This aligns with our intuitive expectation; more precise measurements imply a smaller value for σ_{ex} and a more strongly-peaked (i.e. more informative) probability distribution. The experimental information, for those nuclei which are not already experimentally measured in 2020 AME [26], is given in the upper-right panel of Fig 1. Clearly the information obtained from the experiment is much larger closer to the valley of stability because we can measure those nuclei with a greater precision. The lower left panel of Fig. 1 shows the value of σ_{th} for nuclei which are accessible from FRIB. Many nuclei far from stability, could in principle strongly constrain theoretical mass models but they cannot be easily created at FRIB.

Presuming that the new mass measurement will result in the predicted value, the information gain for a mass measurement given this estimate of the utility is $D_{\text{KL}}(\sigma_{\text{post}}|\sigma_{\text{th}})$ (see Eq. 2), where σ_{post} represents the uncertainty in the posterior probability distribution. The posterior uncertainty, presuming a product of two Gaussian distributions, is

$$\sigma_{\text{post}} = \left(\frac{1}{\sigma_{\text{th}}^2} + \frac{1}{\sigma_{\text{exp}}^2} \right)^{-1/2}, \quad (5)$$

and increases farther away from stability. The larger the value of σ_{ex} , the less information is gained from measuring the mass of a particular nucleus. Eq. 5 ensures that an experimental measurement never decreases our knowledge of a nucleus; σ_{post} is always smaller than σ_{th} .

The value of D_{KL} is plotted in the lower right panel of Fig 1. The nuclei with the largest D_{KL} represent the mass measurements which provide the most information relative to theoretical mass models which attempt to fit the entire mass chart. Note that, for the tabulated nuclei with the largest values of D_{KL} , we found $\sigma_{\text{ex}} \gg \sigma_{\text{th}}$ so $\sigma_{\text{ex}} \approx \sigma_{\text{post}}$, but this is not true in for all of the isotopes in our data set.

Isotope	Z	N	σ_{ex}	σ_{th}	σ_{post}	D_{KL}
^{42}Si	14	28	3.94×10^{-4}	2.78	3.94×10^{-4}	8.36
^{41}Si	14	27	3.82×10^{-4}	2.63	3.82×10^{-4}	8.34
^{43}P	15	28	4.01×10^{-4}	2.39	4.01×10^{-4}	8.19
^{45}S	16	29	4.19×10^{-4}	2.30	4.19×10^{-4}	8.11
^{50}Ar	18	32	4.92×10^{-4}	2.66	4.92×10^{-4}	8.10
^{47}Cl	17	30	4.41×10^{-4}	2.33	4.41×10^{-4}	8.07
^{49}Ar	18	31	4.58×10^{-4}	2.29	4.58×10^{-4}	8.02
^{44}P	15	29	5.94×10^{-4}	2.51	5.94×10^{-4}	7.85
^{46}S	16	30	6.42×10^{-4}	2.63	6.42×10^{-4}	7.82
^{59}Ti	22	37	5.62×10^{-4}	1.77	5.62×10^{-4}	7.56
^{76}Ni	28	48	7.08×10^{-4}	2.11	7.08×10^{-4}	7.50
^{77}Ni	28	49	8.19×10^{-4}	2.41	8.19×10^{-4}	7.49
^{72}Fe	26	46	6.93×10^{-4}	1.92	6.93×10^{-4}	7.43
^{67}Mn	25	42	6.26×10^{-4}	1.69	6.26×10^{-4}	7.40
^{75}Ni	28	47	6.98×10^{-4}	1.88	6.98×10^{-4}	7.40
^{71}Fe	26	45	6.64×10^{-4}	1.75	6.64×10^{-4}	7.38
^{65}Cr	24	41	6.59×10^{-4}	1.67	6.59×10^{-4}	7.34
^{73}Co	27	46	6.89×10^{-4}	1.74	6.89×10^{-4}	7.34
^{70}Fe	26	44	6.53×10^{-4}	1.65	6.53×10^{-4}	7.33
^{68}Mn	25	43	6.97×10^{-4}	1.73	6.97×10^{-4}	7.31

TABLE I. The maximum information gain for experimental nuclear mass measurements relative to the information in theoretical mass models, as measured by the KL divergence.

These results are also summarized in Table I, where the ten nuclei with the largest values of D_{KL} are, in order, ^{42}Si , ^{41}Si , ^{43}P , ^{67}Mn , ^{59}Ti , ^{44}P , ^{77}Ni , ^{45}S , ^{68}Mn , and ^{47}Cl . The properties of the FRIB instrumentation dominate the information gain, because Table I shows that the largest value of D_{KL} is strongly correlated with the smallest value of σ_{ex} . The more accurate the experiment, the more information we gain. However, there are exceptions to this rule. The nucleus with the minimum value of σ_{ex} , ^{41}Si , is not the nucleus with the maximum value of D_{KL} , ^{42}Si . This occurs when σ_{th} is sufficiently large, for nearly equal values of σ_{ex} . In this case, the theoretical uncertainty for ^{42}Si is larger because theoretical models have a difficult time accurately describing the $N = 28$ closed shell. When σ_{ex} is nearly equal between two nuclei, we gain the most information by measuring the nucleus with the larger theoretical uncertainty, i.e. a larger value of σ_{th} . Both the properties of the FRIB facility and the theoretical mass models impact the information gain, but because the range of values of σ_{ex} is much larger than the range of values of σ_{th} , the properties of the FRIB facility have the strongest impact. This is not necessarily the case with the r-process results we show below.

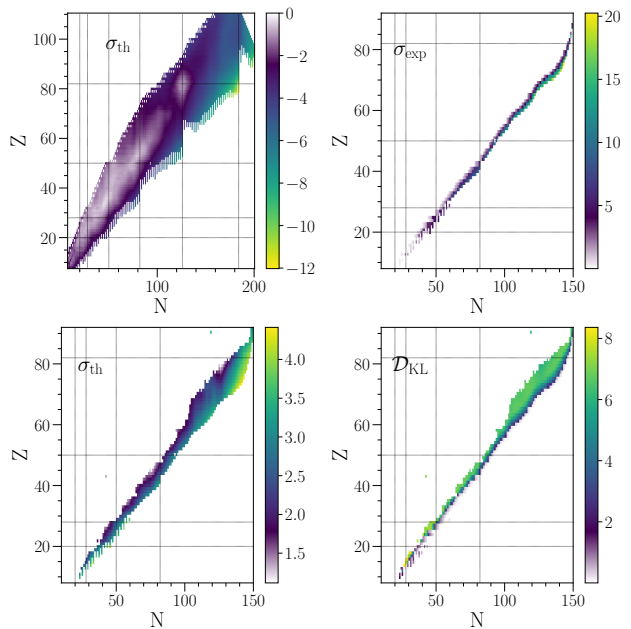


FIG. 1. The top-left panel shows the standard deviation of the theoretical mass model predictions over all nuclei contained in all of the models used in this work. The upper-right panel shows the anticipated uncertainty obtained in an FRIB mass measurement. The lower-left panel also shows the standard deviation of the theoretical mass model predictions, but now constrained only for those nuclei which are not yet, but could be, measured in FRIB. The lower-right panel shows the KL divergence for a mass measurement of each nucleus. The information obtained is larger as one approaches the valley of stability, except for light nuclei where a more complicated variation in A is shown.

IV. INFORMATION GAIN RELATIVE TO R-PROCESS ABUNDANCES

The rapid neutron capture process, or r-process, is responsible for the heaviest elements in the universe. Under varying astrophysical conditions, nuclei can rapidly capture neutrons, creating heavy isotopes not possible via fusion in stars. The origin of r-process nuclei is not yet understood; experimental mass measurements are critical in determining the astrophysical site of the r-process [27]. Core-collapse supernovae and neutron star mergers may both contribute to the observed r-process abundances [28]. These r-process sites listed have varying physical conditions which lead to different abundance patterns. In core-collapse supernovae, r-process nucleosynthesis occurs in the neutrino-driven wind above the newly-born “protonneutron” star. If this neutrino-driven wind does not move too quickly (i.e. if the dynamical timescale is not too short), then the nuclear reactions maintain a robust $(n, \gamma) \rightleftharpoons (\gamma, n)$ equilibrium, referred to as a “hot wind”. During this hot wind, also occurring at high temperatures as the name suggests, the rapid neutron capture process happens quicker than β^- decay. If the wind moves faster and this equilibrium is not

achieved, and is also at relatively low temperatures, then this scenario is referred to as a “cold wind”, where the neutron capture and β^- decays happen at a comparable rate [29]. In the hot wind scenario, r-process nucleosynthesis may proceed with either a high ($S > 120$) or low ($S < 120$) entropy, which would yield differing peaks in isotope production [30]. Another method for heavy element production is neutron star mergers, but unlike with the winds of a core-collapse supernova, they produce nuclei through fission recycling [31]. This process is dominated by neutron capture and beta decay, and spends almost no time in the $(n, \gamma) \rightleftharpoons (\gamma, n)$ equilibrium phase. The composition is so neutron rich, more so than the other three processes, that it quickly reaches the neutron drip line [32]. We will refer to the high and low entropy hot winds as HEHW and LEHW, respectively, the cold wind as CW, and neutron star mergers as NSM.

In order to study these previously described processes, we must find which experiments will contribute the most knowledge to our current understanding of astrophysical systems. To calculate the theoretical information, we use

$$\sigma_{\text{th}} = F\sigma_0, \quad (6)$$

where F is the integrated absolute difference in isobaric mass fractions between a baseline calculation and calculation with modified input nuclear data, as tabulated in Ref. [30] and $\sigma_0 \equiv 1$ MeV. An arbitrary constant is necessary because there is no unique way of determining which probability distribution one should use to determine the information. However, our results are only weakly-dependent on this choice, because the KL divergence depends only on the ratio $\sigma_{\text{post}}/\sigma_{\text{th}}$.

The most informative nuclei are found by once again using the KL divergence for the four astrophysical processes. These are found using the same KL divergence from Eq. 2 for the LEHW, HEHW, CW, and NSM, with the notation taken in this paper to be as follows for each of the astrophysical processes’ KL divergences: D_{LEHW} , D_{HEHW} , D_{CW} , and D_{NSM} .

The theoretical information for each r-process scenario, using only the nuclei which are both measurable in FRIB and important in determining the r-process abundances, is summarized in Fig. 2. From the point of view of the r-process models from Ref. [30], the nuclei with the largest F values and the smallest theoretical information are ^{134}Cd , ^{136}Sn , ^{130}Pd , and ^{130}Pd for the LEHW, HEHW, CW, and NSM scenarios, respectively. The information gain is summarized in Fig. 3. FRIB can measure nuclei near stability with a smaller uncertainty, so the information gain is not maximized for the nuclei above with the smallest theoretical information but for nearby nuclei closer to stability. The mass measurements which optimize the information gain are ^{133}In , ^{136}Sn , ^{133}In , and ^{133}In for the LEHW, HEHW, CW, and NSM scenarios, respectively.

The values of F from Ref. [30] have an arbitrary normalization, so we cannot quantitatively compare the dif-

Isotope Z	N	σ_{th}	σ_{post}	D_{LEHW}	
^{133}In	49	84	9.44	1.27×10^{-3}	8.41
^{134}In	49	85	9.35	2.16×10^{-3}	7.87
^{134}Cd	48	86	52.4	0.0126	7.83
^{133}Cd	48	85	23.4	5.72×10^{-3}	7.82
^{135}In	49	86	10.5	4.66×10^{-3}	7.22
^{196}Hf	72	124	8.93	4.50×10^{-3}	7.09
^{136}Sn	50	86	2.37	1.32×10^{-3}	7.00
^{128}Ag	47	81	2.22	1.24×10^{-3}	6.99
^{141}Te	52	89	2.18	1.37×10^{-3}	6.88
^{128}Pd	46	82	4.71	4.23×10^{-3}	6.52
^{127}Pd	46	81	1.49	1.44×10^{-3}	6.44
^{130}Ag	47	83	12.5	0.0129	6.38
^{129}Ag	47	82	1.92	2.16×10^{-3}	6.29
^{166}Sm	62	104	1.50	1.82×10^{-3}	6.22
^{137}Sn	50	87	2.17	2.74×10^{-3}	6.18
^{138}Sn	50	88	4.55	5.82×10^{-3}	6.16
^{197}Hf	72	125	4.85	6.29×10^{-3}	6.15
^{156}Ce	58	98	1.29	1.69×10^{-3}	6.14
^{194}Hf	72	122	1.96	2.60×10^{-3}	6.12
^{162}Nd	60	102	1.71	2.33×10^{-3}	6.10

TABLE II. The maximum information gain for experimental nuclear mass measurements relative to the information in the low entropy hot wind r-process astrophysical models, as measured by the KL divergence.

Isotope Z	N	σ_{th}	σ_{post}	D_{HEHW}	
^{136}Sn	50	86	83.7	1.32×10^{-3}	10.6
^{133}In	49	84	74.6	1.27×10^{-3}	10.5
^{134}In	49	85	72.8	2.16×10^{-3}	9.93
^{135}In	49	86	73.8	4.66×10^{-3}	9.17
^{138}Sb	51	87	19.2	1.30×10^{-3}	9.10
^{139}Sb	51	88	17.3	1.41×10^{-3}	8.92
^{138}Sn	50	88	29.6	5.82×10^{-3}	8.04
^{136}In	49	87	71.0	0.0154	7.93
^{196}Hf	72	124	13.7	4.50×10^{-3}	7.52
^{141}Te	52	89	4.13	1.37×10^{-3}	7.51
^{140}Sb	51	89	14.1	4.70×10^{-3}	7.51
^{128}Ag	47	81	3.51	1.24×10^{-3}	7.45
^{165}Sm	62	103	4.04	1.61×10^{-3}	7.32
^{167}Eu	63	104	3.95	1.59×10^{-3}	7.32
^{194}Hf	72	122	5.74	2.60×10^{-3}	7.20
^{197}Ta	73	124	5.31	2.46×10^{-3}	7.18
^{166}Sm	62	104	3.77	1.82×10^{-3}	7.14
^{197}Hf	72	125	12.1	6.29×10^{-3}	7.06
^{170}Gd	64	106	2.98	1.63×10^{-3}	7.01
^{168}Eu	63	105	3.17	1.75×10^{-3}	7.00

TABLE III. The maximum information gain for experimental nuclear mass measurements relative to the information in the high entropy hot wind r-process astrophysical models, as measured by the KL divergence.

Isotope Z	N	σ_{th}	σ_{post}	D_{CW}	
^{133}In	49	84	4.20	1.27×10^{-3}	7.60
^{141}Te	52	89	3.44	1.37×10^{-3}	7.33
^{134}In	49	85	4.12	2.16×10^{-3}	7.05
^{143}I	53	90	1.38	1.34×10^{-3}	6.43
^{128}Ag	47	81	1.23	1.24×10^{-3}	6.40
^{142}Te	52	90	2.22	2.37×10^{-3}	6.34
^{138}Sb	51	87	0.89	1.30×10^{-3}	6.03
^{136}Sn	50	86	0.89	1.32×10^{-3}	6.02
^{139}Sb	51	88	0.85	1.41×10^{-3}	5.90
^{130}Pd	46	84	43.7	0.0776	5.83
^{129}Ag	47	82	1.18	2.16×10^{-3}	5.80
^{135}In	49	86	2.32	4.66×10^{-3}	5.71
^{126}Pd	46	80	0.60	1.21×10^{-3}	5.71
^{128}Pd	46	82	1.91	4.23×10^{-3}	5.61
^{167}Eu	63	104	0.67	1.59×10^{-3}	5.54
^{134}Cd	48	86	5.17	0.0126	5.52
^{194}Hf	72	122	1.03	2.60×10^{-3}	5.48
^{192}Hf	72	120	0.71	1.82×10^{-3}	5.47
^{154}Ce	58	96	0.55	1.46×10^{-3}	5.43
^{193}Hf	72	121	0.71	1.97×10^{-3}	5.39

TABLE IV. The maximum information gain for experimental nuclear mass measurements relative to the information in the cold wind r-process astrophysical models, as measured by the KL divergence.

Isotope Z	N	σ_{th}	σ_{post}	D_{NSM}	
^{133}In	49	84	6.07	1.27×10^{-3}	7.97
^{134}In	49	85	5.92	2.16×10^{-3}	7.42
^{128}Ag	47	81	2.89	1.24×10^{-3}	7.26
^{126}Pd	46	80	2.46	1.21×10^{-3}	7.12
^{127}Ag	47	80	1.68	1.18×10^{-3}	6.76
^{129}Ag	47	82	2.90	2.16×10^{-3}	6.70
^{127}Pd	46	81	1.85	1.44×10^{-3}	6.66
^{124}Pd	46	78	1.34	1.16×10^{-3}	6.56
^{126}Ag	47	79	1.28	1.17×10^{-3}	6.49
^{141}Te	52	89	1.46	1.37×10^{-3}	6.47
^{128}Pd	46	82	3.06	4.23×10^{-3}	6.08
^{125}Pd	46	79	0.71	1.17×10^{-3}	5.91
^{143}I	53	90	0.63	1.34×10^{-3}	5.65
^{142}Te	52	90	1.05	2.37×10^{-3}	5.59
^{192}Hf	72	120	0.66	1.82×10^{-3}	5.39
^{193}Hf	72	121	0.70	1.97×10^{-3}	5.38
^{194}Hf	72	122	0.91	2.60×10^{-3}	5.36
^{130}Pd	46	84	24.2	0.0776	5.24
^{135}In	49	86	1.45	4.66×10^{-3}	5.24
^{154}Ce	58	96	0.45	1.46×10^{-3}	5.23

TABLE V. The maximum information gain for experimental nuclear mass measurements relative to the information in the neutron star merger r-process astrophysical models, as measured by the KL divergence.

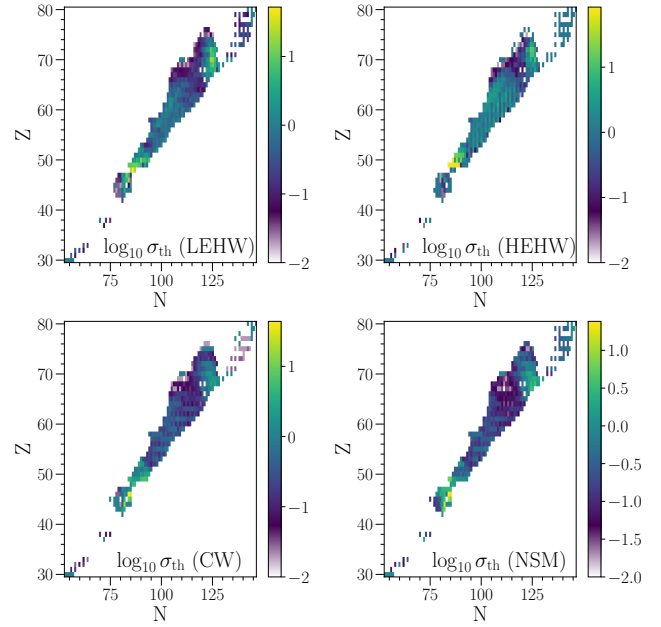


FIG. 2. Log of theoretical standard deviation for low entropy hot wind (top left). Log of theoretical standard deviation for high entropy hot wind (top right). Log of theoretical standard deviation for cold wind (bottom left). Log of theoretical standard deviation for neutron star mergers (bottom right). Nuclei in yellow represent the largest standard deviation, while nuclei with a smaller standard deviation are colored light purple.

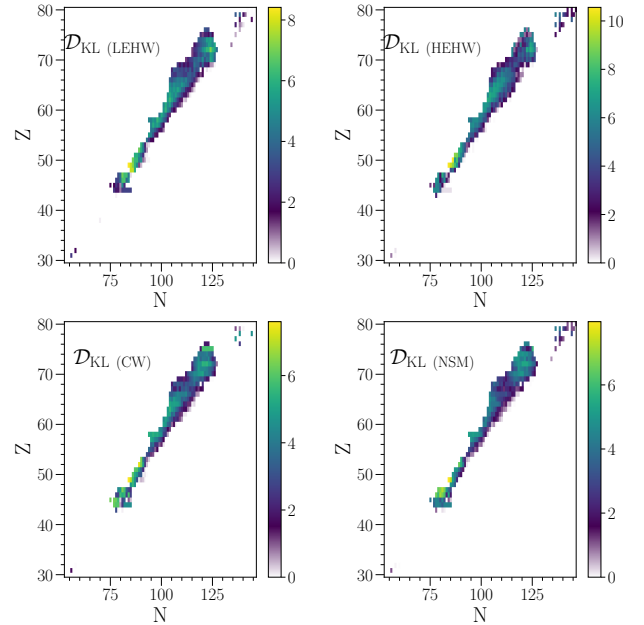


FIG. 3. KL divergence for low entropy hot wind (top left). KL divergence for high entropy hot wind (top right). KL divergence for cold wind (bottom left). KL divergence for neutron star mergers (bottom right). Nuclei in yellow represent the greatest information gain, while less informative nuclei are colored light purple.

ferent r-process scenarios with each other. Our formalism only allows one to determine the most informative mass measurements within one of the four scenarios. Nevertheless, it appears that some nuclei, like ^{133}In and ^{134}In are important masses to measure independent of which r-process scenario is closer to reality.

For D_{KL} relative to r-process abundances, the theoretical standard deviation has more of an impact than the experimental standard deviation. This is in contrast to D_{KL} relative to theoretical nuclear mass models, where the theoretical standard deviation had very little impact in D_{KL} . The origin of this effect is that the F-values found in Ref. [30] have a much larger range of four orders of magnitude, (0.01 to 101.39), as compared to the range of uncertainties in the theoretical nuclear mass models from the previous section (only a factor four). Since the F values cover a wider range, they have more of an ability to impact the final value of D_{KL} . This can be seen by comparing the the top right panel of Fig. 1 and each panel of Fig. 2 with each panel in Fig. 3. Fig. 2 and Fig. 3 have the same general shape, while σ_{ex} from Fig. 1 has some, but less of an impact on D_{KL} . This follows for the most part, unless σ_{ex} is very small compared to σ_{th} , as in ^{134}Cd . ^{134}Cd appears in tables II and IV with a significantly larger σ_{th} than any other nucleus, but is overshadowed by the small σ_{ex} of ^{133}In , so there is a balance between these two values.

While this work was being completed, the ^{133}In mass was measured [33]. The next most informative measurement depends on the most likely r-process scenario, though clearly the ($Z = 50, N = 82$) region of the periodic table is a source of many informative mass measurements.

V. DISCUSSION AND CONCLUSION

For FRIB to make the most out of their resources, D_{KL} should be as large as possible. This means that for D_{KL} relative to theoretical mass models, the experimental information is large compared to the theoretical information. In contrast, if the theoretical information is large, regardless of the size of the experimental information, D_{KL} will be small due to having a large uncertainty in the theoretical models. If σ_{ex} is small, regardless of

the size of the theoretical information, D_{KL} will be large, simply due to the fact that there is a lot of information to gain. The least uncertainty and therefore most information gain will occur in the latter scenario, where σ_{ex} is small.

For D_{KL} relative to r-process abundances, the theoretical information has more of an impact than the experimental. This is due to having a larger range of theory values for the r-process abundances as compared to the theoretical mass models. Both σ_{ex} and σ_{th} do have an impact on D_{KL} , and the nuclei with the largest values of D_{KL} in all four astrophysical scenarios occur when both σ_{ex} and σ_{th} are small.

Our method for computing the KL divergence relative to the theoretical mass models presumes that the new mass measurement will be equal to the value predicted by theory. We have averaged over the theoretical mass models in order to attempt to suppress our dependence on the systematics of any one mass formula. However, if it is determined that many of the mass predictions suffer from the same systematic flaw, then this will impact the result.

In the future, facilities could utilize this function to their advantage. Ideally, after each nucleus at a given facility is studied, it is added to the experimental model, and this calculation is performed again. This would allow for the most accurate measurements of D_{KL} given the most up to date experimental measurements. Using this model, facilities worldwide could collaborate and nuclear physics could be studied at the most efficient rate possible.

ACKNOWLEDGMENTS

JNF and AWS were supported by NSF grants PHY 1554876. ZM was supported in part by the U.S. Department of Energy under Grants No. DE-FG02-88ER40387, No. DE-NA0003909, and No. DE-SC0019042. ZM also benefited from support by the National Science Foundation under Grant No. PHY-1430152 (JINA Center for the Evolution of the Elements). AWS was additionally supported by NSF grant PHY 2116686 and the U.S. DOE Office of Nuclear Physics.

-
- [1] M. Redshaw, G. Bollen, S. Bustabad, A. A. Kwiatkowski, D. L. Lincoln, S. J. Novario, R. Ringle, S. Schwarz, and A. A. Valverde, Nucl. Instrum. Meth. B **317**, 510 (2013).
 - [2] D. Lunney, J. M. Pearson, and C. Thibault, Reviews of Modern Physics **75**, 1021 (2003).
 - [3] G. Bollen, Nuc. Phys. A **693**, 3 (2001).
 - [4] J. K. Tuli, Tech. Rep., National Nuclear Data Center (2011), 8th Edition.
 - [5] P. Möller, B. Pfeiffer, and K.-L. Kratz, Phys. Rev. C **67**, 055802 (2003).
 - [6] Z. Meisel, S. George, S. Ahn, D. Bazin, B. A. Brown, J. Browne, J. F. Carpino, H. Chung, R. H. Cyburt, A. Estradé, et al., Phys. Rev. C **101**, 052801(R) (2020).
 - [7] Z. Meisel, Journal of Physics: Conference Series **1668**, 012026 (2020), URL <https://doi.org/10.1088/1742-6596/1668/1/012026>.
 - [8] G. Bollen, M. Hausmann, B. M. Sherrill, and O. B. Tarasov, FRIB Estimated Rates v1.06 (2011).
 - [9] N. Chamel, S. Goriely, and J. M. Pearson, Phys. Rev. C **80**, 065804 (2009), URL <https://link.aps.org/doi/>

- 10.1103/PhysRevC.80.065804.
- [10] J. Duflo and A. Zuker, Phys. Rev. C **52**, R23 (1995), URL <https://link.aps.org/doi/10.1103/PhysRevC.52.R23>.
- [11] J.-P. Ebran, E. Khan, D. Peña Arteaga, and D. Vretenar, Phys. Rev. C **83**, 064323 (2011), URL <https://link.aps.org/doi/10.1103/PhysRevC.83.064323>.
- [12] S. Goriely, M. Samyn, M. Bender, and J. M. Pearson, Phys. Rev. C **68**, 054325 (2003), URL <https://link.aps.org/doi/10.1103/PhysRevC.68.054325>.
- [13] S. Goriely and J. M. Pearson, Phys. Rev. C **77**, 031301 (2008), URL <https://link.aps.org/doi/10.1103/PhysRevC.77.031301>.
- [14] S. Goriely, M. Samyn, and J. M. Pearson, Phys. Rev. C **75**, 064312 (2007), URL <https://link.aps.org/doi/10.1103/PhysRevC.75.064312>.
- [15] S. Goriely, N. Chamel, and J. M. Pearson, Phys. Rev. C **82**, 035804 (2010), URL <https://link.aps.org/doi/10.1103/PhysRevC.82.035804>.
- [16] S. Goriely, S. Hilaire, and A. J. Koning, Phys. Rev. C **78**, 064307 (2008), URL <https://link.aps.org/doi/10.1103/PhysRevC.78.064307>.
- [17] S. Goriely and R. Capote, Phys. Rev. C **89**, 054318 (2014), URL <https://link.aps.org/doi/10.1103/PhysRevC.89.054318>.
- [18] H. Koura, T. Tachibana, M. Uno, and M. Yamada, Progr. Theor. Phys. **113**, 305 (2005), URL <https://doi.org/10.1143/PTP.113.305>.
- [19] W. H. Long, P. Ring, N. V. Giai, and J. Meng, Phys. Rev. C **81**, 024308 (2010), URL <https://link.aps.org/doi/10.1103/PhysRevC.81.024308>.
- [20] M. Liu, N. Wang, Y. Deng, and X. Wu, Phys. Rev. C **84**, 014333 (2011).
- [21] P. Möller, A. Sierk, T. Ichikawa, and H. Sagawa, Atomic Data and Nuclear Data Tables **109-110**, 1 (2016), ISSN 0092-640X, URL <https://doi.org/10.1016/j.adt.2015.10.002>.
- [22] J. M. Pearson, S. Goriely, and N. Chamel, Phys. Rev. C **83**, 065810 (2011), URL <https://link.aps.org/doi/10.1103/PhysRevC.83.065810>.
- [23] P. K. Rath, R. Chandra, K. Chaturvedi, P. K. Raina, and J. G. Hirsch, Phys. Rev. C **82**, 064310 (2010), URL <https://link.aps.org/doi/10.1103/PhysRevC.82.064310>.
- [24] N. Wang, M. Liu, and X. Wu, Phys. Rev. C **81**, 044322 (2010).
- [25] N. Wang, Z. Liang, M. Liu, and X. Wu, Phys. Rev. C **82**, 044304 (2010).
- [26] W. J. Huang, M. Wang, F. G. Kondev, G. Audi, and S. Naimi, Chin. Phys. C **45**, 030002 (2021), URL <https://doi.org/10.1088/1674-1137/abddb0>.
- [27] J. J. Cowan and F.-K. Thielemann, Physics Today pp. 47–53 (2004).
- [28] F. Thielemann, A. Arcones, R. Käppeli, M. Liebendörfer, T. Rauscher, C. Winteler, C. Fröhlich, I. Dillmann, T. Fischer, . Martinez-Pinedo, G., et al., **66**, 346 (2011), URL <https://doi.org/10.1016/j.ppnp.2011.01.032>.
- [29] A. Arcones and G. Martínez-Pinedo, Physical Review C **83** (2011), ISSN 1089-490X, URL <http://dx.doi.org/10.1103/PhysRevC.83.045809>.
- [30] M. R. Mumpower, R. Surman, G. C. McLaughlin, and A. Aprahamian, Prog. Part. Nucl. Phys. **86**, 86 (2016), URL <https://doi.org/10.1016/j.ppnp.2015.09.001>.
- [31] D. Yong, C. Kobayashi, G. Da Costa, M. Bessell, A. Chiti, A. Frebel, K. Lind, A. Mackey, T. Nordlander, M. Asplund, et al., Nature (2021), URL <https://www.nature.com/articles/s41586-021-03611-2>.
- [32] B. Côté, M. Eichler, A. Arcones, C. J. Hansen, P. Simonetti, A. Frebel, C. L. Fryer, M. Pignatari, M. Reichert, K. Belczynski, et al., The Astrophysical Journal **875**, 106 (2019), ISSN 1538-4357, URL <http://dx.doi.org/10.3847/1538-4357/ab10db>.
- [33] C. Izzo, J. Bergmann, K. A. Dietrich, E. Dunling, D. Fusco, A. Jacobs, B. Kootte, G. Kriepkó-Koncz, Y. Lan, E. Leistenschneider, et al., Phys. Rev. C **103**, 025811 (2021), URL <https://link.aps.org/doi/10.1103/PhysRevC.103.025811>.